

Received January 7, 2019, accepted February 1, 2019, date of publication February 14, 2019, date of current version March 25, 2019.

Digital Object Identifier 10.1109/ACCESS.2019.2897711

Modified Quasi-Newton Optimization Algorithm-Based Iterative Learning Control for Multi-Axial Road Durability Test Rig

XIAO WANG¹, DACHENG CONG¹, ZHIDONG YANG¹, SHENGJIE XU², AND JUNWEI HAN¹

¹State Key Laboratory of Robotics and System, Harbin Institute of Technology, Harbin 150001, China

²China Automotive Technology and Research Center, Tianjin 300300, China

Corresponding author: Zhidong Yang (yangzhidong@hit.edu.cn)

This work was supported in part by the National Natural Science Foundation of China under Grant 51205077.

ABSTRACT The iterative learning control (ILC) based on the linear frequency-domain model has been employed to replicate the road conditions for the vehicle durability testing in the laboratory. Generally, the vehicle and the multi-axial hydraulic test rig behave strong nonlinearities, which requires a large number of iterations to correct the tracking error. Hence, the process of drive file (i.e., the input signals which drive the actuators of the test rig) generation is time-lengthy and tedious. A method that combines the ILC with the Quasi-Newton algorithm over the complex space (QNLIC) is developed to speed up the drive file construction for the multi-axial vibration test rig. The impedance matrix can be updated with Broyden's method to reduce the modeling errors and make the iteration more robust. An auxiliary estimating loop is inserted into the iteration process to attain an optimal learning gain. The convergence of the proposed method has been proven to be monotonic. This approach is validated through simulation, where the target signals are the real-life spindle forces gathered from the wheel force transducer. The simulation results demonstrate that the QNLIC can improve the convergence rate and increase the tracking accuracy than the current offline ILC. The QNLIC reduces the iteration number from nine down to five to converge to the desirable index compared with the offline ILC using gain 0.5. The new method based on the optimization algorithm can extend to other repetitive tracking processes.

INDEX TERMS Road durability testing, iterative learning control, Broyden's method, optimal learning gain, the multi-axial road test rig.

I. INTRODUCTION

Within the automotive industry, service load simulation in the laboratory is indispensable in the vehicle development to access its durability. Usually, the lab simulation is implemented with the multi-axial hydraulic test rigs [1]. The main advantages of laboratory testing are that it cannot be limited by the driver's skill and traffic and weather conditions and can reduce running time and cost with an accelerated vibration test method [2].

It is essential to reproduce the service loads accurately to respond to the realistic vibration environment and the state-of-the-art technique for automotive durability testing is the offline Iterative Learning Control (ILC) [3]. In this method,

The associate editor coordinating the review of this manuscript and approving it for publication was Luigi Biagiotti.

a linear Frequency Response Function (FRF) matrix is identified experimentally. However, the nonlinear characteristics of the hydraulic test rig with the vehicle under test make the approach yield tracking errors so that a high number of iterations are unavoidable to correct it, which becomes time-consuming and onerous for the operators and increases the risk of specimen damage. As a consequence, it has great value to improve the convergence rate of iteration [4].

Many researchers have worked to speed up the convergence properties of iteration from different aspects. In order to obtain a more precise FRF model, several FRF models with the coherence functions as weights are averaged [5] and different excitation signals are also tried to improve the identification accuracy [6]. The simulation channels are optimized for the inverse FRF calculation on a six-axis road load simulator [7]. An adaptive modeling procedure based

on the forward prediction method is developed to update the FRF model for compensating the modeling error during the iterations [8], but it requires the system to be weakly-coupled. Musella U etc [9] applied the CR-Calculus to update the FRF matrix for random vibration control.

In lieu of the usual frequency domain implementation, Raath [10] firstly described the system with the parametric time domain model for road simulation. De Cuyper and Verhaegen [11] also identified an industrial seat test rig with state space models and inverted the obtained models with the Stable Dynamic Inversion (SDI) method. The Autoregressive Moving Average Model with the exogenous inputs (ARMAX) model [12] and the Autoregressive Model with exogenous inputs (ARX) [13]–[15] are applied to the ILC. The Adaptive Inverse Plant Modeling (AIPM) technique is used by Moten *et al.* [16] to identify the system. The NARX model-based ILC also has been presented in several literature [17]–[20]. The parametric model can use shorter measurement data to be identified, but it is laborious to choose a reasonable order and structure for each part of the multi-variable model [14], [15]. The parametric model based ILC method is more suited to smaller numbers of channels [10] to be a supplement to the classical ILC. Besides, the iteration gains in most recent work are still chosen manually to avoid destabilization of the iteration process, which cannot guarantee the monotonic convergence.

The offline ILC scheme is augmented with a real-time H_∞ feedback proposed by De Cuyper [21] and De Cuyper *et al.* [22] or with modified internal model controller developed by Tang [23] to promote the convergence rate. But the design of extra controllers is burdensome for every component under test especially for the multi-axis testing.

The Norm Optimal ILC (NOILC) [24] as well as Parameter Optimal ILC (POILC) [25] have been proposed. In addition, the ILC can be combined with the Newton method [26], Quasi-Newton method [27]. But the above-mentioned methods are not suitable for the long duration testing because they are deduced in the time domain and input and output signal vectors are usually super-vectors [28].

All above efforts have facilitated the development of drive file generation. It is still challenging to pursue the more suitable approach for multi-axis road simulation testing. The CGILC method has been studied by wang *et al.* [29]. This method converges very fast at the first iteration steps, but the convergence rate suffers from the couplings more severely. The Quasi-Newton (QN) method is usual to solve nonlinear optimization problems [30]. The optimization over complex space has been studied and applied in engineering such as communications [31]. In this work, the method embedding the QN method over complex space into the conventional offline ILC (QNILC) is studied for durability testing.

This paper is organized as follows. Section 2 describes the experimental multi-axis test rig. Section 3 summarizes the classical offline ILC method in automotive industry. Section 4 presents optimization theory over complex space and the



FIGURE 1. Quarter car suspension test rig.

theory of QNILC and proves the convergence of this method to be monotonic. Section 5 is devoted to verifying the performance of the QNILC and discussing the simulation results. Finally, the conclusions of the paper are given in Section 6.

In the following part, the vectors are denoted with the lower case bold letters (e.g. \mathbf{u}) and matrices with the upper case bold letters (e.g. \mathbf{G}). In section 3 and 4 the variables all depend on the angular frequency ω [rad/s] without specification.

II. EXPERIMENTAL MULTI-AXIAL SUSPENSION TEST RIG

The layout of one corner of the MTS 329 spindle-coupled test rig where a front suspension is mounted can be seen in Figure 1. This suspension test rig allows the simulation of the forces and moments, hence six degrees of freedom at each spindle [21].

The suspension test rig is typically a Multiple-Input Multiple-Output (MIMO) system with parameter uncertainties, which come from the mechanical coupling, non-linear hydraulic valve displacement, dynamic loading change and the variance of supply oil pressure [2]. The nonlinearities of suspension reside in the damper, bushings and bump-stop.

In Figure 2, a McPherson suspension is mounted on the fixture and the hydraulic test rig is controlled by the PID controller [21]. In practice, the PID controller is usual in the vehicle durability testing [6], [14]. Due to the frequent replacement of specimen in the durability testing, the PID controller is more suitable and easy to tune. With the data acquired from this system, the simulation model is established to replace the real physical test rig. The proposed method can be validated through this approximate model and moreover, the commercial suspension can be free from being damaged unexpectedly.

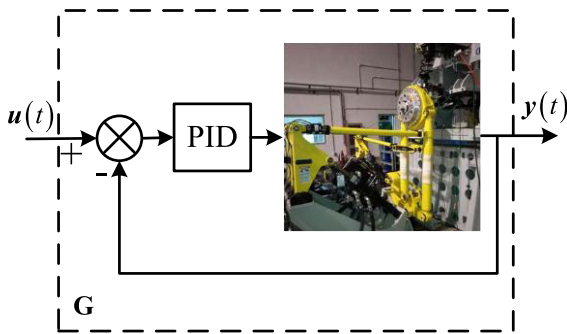


FIGURE 2. The servo-hydraulic system with the PID controller.

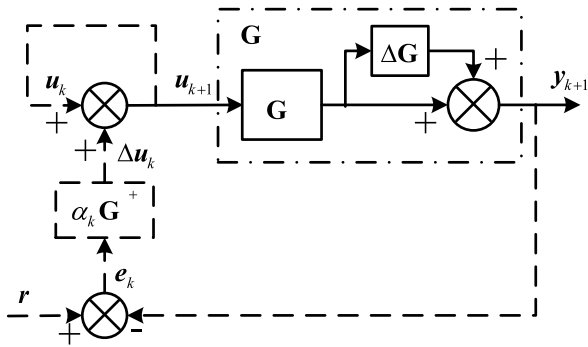


FIGURE 3. The classical off-line iteration.

III. CLASSICAL OFFLINE ITERATION LEARNING CONTROL

The classical offline ILC exists in the commercial software, such as RPC (Remote Parameter Control) of MTS Corporation and TWR (Time Waveform Replication) of Siemens [1]. All these systems use the same fundamental mathematical approach summarized in following part.

In Fig. 3, $G \in \mathbb{C}^{M \times N}$ represents the actual closed-loop system, which can be expressed with the identified system model \hat{G} and the difference ΔG between the estimated model and the actual system.

The targets, the measured responses and the drives are denoted with $r(t) = \{r_1(t), \dots, r_N(t)\}^T$, $y(t) = \{y_1(t), \dots, y_M(t)\}^T$ and $u(t) = \{u_1(t), \dots, u_N(t)\}^T$, respectively. The spectral analysis uses the Discrete Fourier Transform of these signals.

The system shown in Figure 2 can be given by

$$y = Gu = \hat{G}(I + \Delta G)u \quad (1)$$

where $u \in \mathbb{C}^{N \times 1}$ and $y \in \mathbb{C}^{M \times 1}$ are spectra of drive signals and measured responses, respectively.

Figure 3 illustrates the detailed classical ILC approach. It is composed of two main aspects: System Identification and Target Simulation [3]. Firstly, the H_1 method is applied to calculate the FRF matrix \hat{G} .

Taking the inverse of the FRF matrix \hat{G} based on the Singular Value Decomposition (SVD), the mechanical impedance matrix is obtained

$$\hat{Z} = \hat{G}^+ \quad (2)$$

where the superscript $+$ presents the Moore-Penrose pseudo-inverse.

In the second phase, the drives are optimized with the impedance matrix iteratively according to

$$u_{k+1} = u_k + \alpha_k \hat{G}^+ (r - y_k) = u_k + \alpha_k \hat{Z} e_k \quad k = 0, 1, 2, 3 \dots \quad (3)$$

where α_k is the k th learning gain, satisfying $0 \leq \alpha_k \leq 1$

In industrial practice, the test rig with the suspension under test behaves strongly non-linear, causing significant modeling errors [1]. In this case, a conservative small learning gain should be adopted to keep convergence but requires more iterations. In practice, the gain is generally chosen manually with the iterations.

IV. THE OFFLINE ILC STRATEGY WITH QUASI-NEWTON OPTIMIZATION ALGORITHM

A. THE OPTIMIZATION PRINCIPLE OVER THE COMPLEX SPACE

The iterative control problem can be seen as an optimization problem, i.e. to find the minimum of a function [32].

The gradient-based approach over the complex space has been proposed [33]. Given $z \in \mathbb{C}^{N \times 1}$, then define $\bar{z} = \begin{bmatrix} z \\ z^* \end{bmatrix}$. The complex conjugate, the complex conjugate transpose as well as the transpose are denoted with the superscript $*$, $.^H$ and $.^T$, respectively. A real scalar-valued function about \bar{z} can be expressed as [33]

$$f(\bar{z})f(z, z^*), \mathbb{C}^{2N} \rightarrow \mathbb{R} \quad (4)$$

The second-order Taylor expansion of $f(\bar{z})$ yields [33]

$$f(\bar{z} + \Delta \bar{z}) = f(\bar{z}) + \Delta \bar{z}^T \frac{\partial f(\bar{z})}{\partial \bar{z}} + \frac{1}{2} \Delta \bar{z}^H \frac{\partial^2 f(\bar{z})}{\partial \bar{z}^* \partial \bar{z}^T} \Delta \bar{z} \quad (5)$$

The complex gradient can be given by [33]

$$\frac{\partial f(\bar{z} + \Delta \bar{z})}{\partial \Delta \bar{z}^*} = \frac{\partial f(\bar{z})}{\partial \bar{z}^*} + \frac{\partial^2 f(\bar{z})}{\partial \bar{z}^* \partial \bar{z}^T} \Delta \bar{z} = \nabla f(\bar{z}) + \nabla^2 f(\bar{z}) \Delta \bar{z} \quad (6)$$

where $\nabla f(\bar{z})$ is the gradient vector and $\nabla^2 f(\bar{z})$ is the Hessian matrix.

Finding the minimum of Equation (4) leads the Equation (6) to be 0. So expanding the Equation (6), the following relation should be satisfied [34]

$$\begin{bmatrix} \frac{\partial^2 f(\bar{z})}{\partial z^* \partial z^T} & \left(\frac{\partial^2 f(\bar{z})}{\partial z \partial z^T} \right)^* \\ \frac{\partial^2 f(\bar{z})}{\partial z \partial z^T} & \frac{\partial^2 f(\bar{z})}{\partial z \partial z^H} \end{bmatrix} \begin{bmatrix} \Delta z \\ \Delta z^* \end{bmatrix} = \begin{bmatrix} -\frac{\partial f(\bar{z})}{\partial z^*} \\ -\frac{\partial f(\bar{z})}{\partial z} \end{bmatrix} \quad (7)$$

Assuming $\frac{\partial^2 f(\bar{z})}{\partial z \partial z^T} = 0$, then Δz can be derived

$$\Delta z = - \left(\frac{\partial^2 f(\bar{z})}{\partial z^* \partial z^T} \right)^{-1} \frac{\partial f(\bar{z})}{\partial z^*} \quad (8)$$

When the drive vectors reach the optimum, the tracking error e will be zero. If $\frac{\partial^2 f(\bar{z})}{\partial z \partial z^T} = \left(\frac{\partial^2 f(\bar{z})}{\partial z^* \partial z^T} \right)^* = 0$, the invertibility of $\frac{\partial^2 f(\bar{z})}{\partial z^* \partial z^T}$ is a necessary and sufficient condition for a solution \bar{z} to exist [35]. Also, the assumption can improve the numerical robustness of the Newton algorithm and provide a substantial simplification [35].

The Newton's method leads to the following iteration

$$z_{k+1} = z_k + \Delta z_k = z_k - \left(\frac{\partial^2 f(\bar{z}_k)}{\partial z_k^* \partial z_k^T} \right)^{-1} \frac{\partial f(\bar{z}_k)}{\partial z_k^*} \quad (9)$$

B. THE ILC BASED ON QUASI-NEWTON ALGORITHM

In this section, the optimization approach over the complex space above is applied to the solution of the optimum drive signal for the road durability test.

The drive \mathbf{u} is determined by minimizing the following real-valued function

$$\min \Gamma(\bar{\mathbf{u}}) \Gamma(\mathbf{u}, \mathbf{u}^*) = \|e\|^2 = (\mathbf{r} - \mathbf{G}\mathbf{u})^H (\mathbf{r} - \mathbf{G}\mathbf{u}), \quad \mathbb{C}^{2N} \rightarrow \mathbb{R} \quad (10)$$

where $\|\cdot\|$ represents the Euclidean vector norm and $\|\mathbf{v}\| = \sqrt{\langle \mathbf{v}, \mathbf{v} \rangle} = \sqrt{\mathbf{v}^H \mathbf{v}}, \mathbf{v} \in \mathbb{C}^{N \times 1}$.

Assume that the system is independent of the drive signal and the complex conjugate gradient vector is given by

$$\nabla \Gamma = \frac{\partial \Gamma(\bar{\mathbf{u}})}{\partial \mathbf{u}^*} = -\mathbf{G}^H (\mathbf{r} - \mathbf{G}\mathbf{u}) = -\mathbf{G}^H (\mathbf{r} - \mathbf{y}) = -\mathbf{G}^H \mathbf{e} \quad (11)$$

The complex Hessian matrix [36] can be written as

$$\mathbf{H} = \frac{\partial^2 \Gamma(\bar{\mathbf{u}})}{\partial \mathbf{u}^* \partial \mathbf{u}^T} = \mathbf{G}^H \mathbf{G} \quad (12)$$

where \mathbf{H} is a Hermitian positive definite matrix.

According to Equation (8), the search direction \mathbf{d}_k is generated by

$$\mathbf{d}_k = -\mathbf{H}_k^{-1} \nabla \Gamma_k = (\mathbf{G}^H \mathbf{G})^{-1} \mathbf{G}^H \mathbf{e}_k \quad (13)$$

In practice, the physical system model G cannot be acquired exactly so the experimentally identified FRF matrix \hat{G} can substitute for it. Based on Equation (9), the drive can be updated

$$\mathbf{u}_{k+1} = \mathbf{u}_k + \alpha_k \mathbf{d}_k = \mathbf{u}_k + \alpha_k (\hat{\mathbf{G}}^H \hat{\mathbf{G}})^{-1} \hat{\mathbf{G}}^H \mathbf{e}_k = \mathbf{u}_k + \alpha_k \hat{\mathbf{Z}} \mathbf{e}_k \quad (14)$$

It is obvious that the classical offline ILC method is a particular example of optimization problem.

If the modeling errors can be reduced, the ILC procedure can be made more robust, i.e. it is more likely to increase the convergence rate. But re-identifying the FRF matrix after each iteration is cumbersome. On the real test rig, some attempts [6], [37] have been made to improve the ILC convergence properties by updating the FRF matrix. In practice, unknown disturbances and modeling errors prevent the ILC to be successful [37]. In this work, the impedance matrix will be

updated iteratively with the Broyden's method in the Quasi-Newton algorithm to correct the errors that remain.

Apply the Broyden's method to update the inverse Hessian matrix, which is expressed as [38], [39]

$$\mathbf{H}_{k+1}^{-1} = \mathbf{H}_k^{-1} + \frac{(\mathbf{s}_k - \mathbf{H}_k^{-1} \mathbf{g}_k) \mathbf{s}_k^H}{\langle \mathbf{H}_k^{-1} \mathbf{g}_k, \mathbf{s}_k \rangle} \mathbf{H}_k^{-1} \quad (15)$$

where \mathbf{s}_k and \mathbf{g}_k denote the variation of the drive signal and the gradient, respectively.

$$\mathbf{s}_k = \mathbf{u}_k - \mathbf{u}_{k-1} = \Delta \mathbf{u}_k \quad (16)$$

$$\begin{aligned} \mathbf{g}_k &= \nabla \Gamma_k - \nabla \Gamma_{k-1} = -\mathbf{G}^H (\mathbf{r} - \mathbf{y}_k) + \mathbf{G}^H (\mathbf{r} - \mathbf{y}_{k-1}) \\ &= \mathbf{G}^H (\mathbf{y}_k - \mathbf{y}_{k-1}) \\ &= \mathbf{G}^H \Delta \mathbf{y}_k \end{aligned} \quad (17)$$

The impedance matrix is calculated with the Moore-Penrose pseudo-inverse and the approximate inverse Hessian matrix can be defined as

$$\mathbf{H}^{-1} = \mathbf{Z} (\mathbf{G}^H)^{-1} \quad (18)$$

Substitute Equation (18) into the Equation (15), the impedance matrix can be updated as

$$\hat{\mathbf{Z}}_{k+1} = \left(\mathbf{I} + \frac{(\mathbf{s}_k - \hat{\mathbf{Z}}_k \Delta \mathbf{y}_k) \mathbf{s}_k^H}{\langle \hat{\mathbf{Z}}_k \Delta \mathbf{y}_k, \mathbf{s}_k \rangle} \right) \hat{\mathbf{Z}}_k \quad (19)$$

To guarantee global convergence, a line search can be conducted to attain an optimal iteration gain, where the merit function about α_k is

$$\min_{\alpha \in \mathbb{C}} \Phi(\bar{\alpha}_k) = \Phi(\alpha_k, \alpha_k^*) = \|\mathbf{r} - \mathbf{G}(\mathbf{u}_k + \alpha_k \mathbf{d}_k)\|^2 \quad (20)$$

If $d\Phi/d\alpha^* = 0$, then yields the learning gain

$$\alpha_k = \frac{(\mathbf{G}\mathbf{d}_k)^H \mathbf{e}_k}{(\mathbf{G}\mathbf{d}_k)^H \mathbf{G}\mathbf{d}_k} = \frac{\langle \mathbf{G}\mathbf{d}_k, \mathbf{e}_k \rangle}{\langle \mathbf{G}\mathbf{d}_k, \mathbf{G}\mathbf{d}_k \rangle} \quad (21)$$

Still, the exact value of α_k cannot be obtained owing to unknown physical model G . The learning gain can be alternatively estimated by inserting an extra loop [40].

The concrete calculation procedure of the optimal learning gain is illustrated in detail in the following.

$$\hat{\mathbf{u}}_{k+1} = \mathbf{u}_k + \lambda \mathbf{d}_k \quad (22)$$

where λ is the step size of estimating loop.

Multiplying two sides of Equation (22) by G yields

$$G\hat{\mathbf{u}}_{k+1} = G\mathbf{u}_k + \lambda G\mathbf{d}_k \quad (23)$$

$$\hat{\mathbf{y}}_{k+1} = \mathbf{y}_k + \lambda G\mathbf{d}_k \quad (24)$$

The increment between the two consecutive responses can be expressed as

$$G\mathbf{d}_k = \frac{1}{\lambda} (\hat{\mathbf{y}}_{k+1} - \mathbf{y}_k) = \frac{1}{\lambda} \hat{\mathbf{e}}_k \quad (25)$$

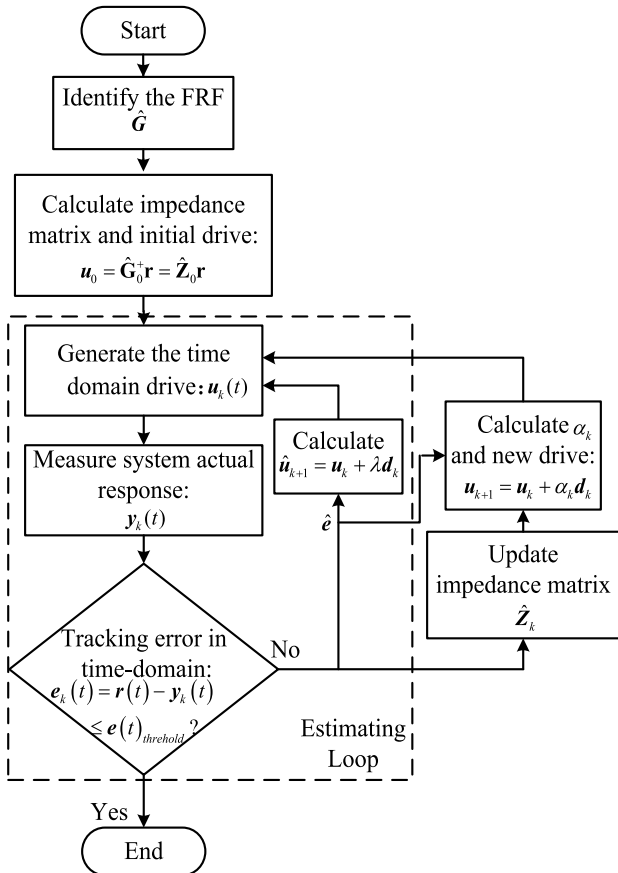


FIGURE 4. The flow chart of QNILC.

Substituting Equation (25) into Equation (21), the learning gain can be reformulated as

$$\alpha_k = \lambda \frac{\langle \hat{\mathbf{e}}_k, \mathbf{e}_k \rangle}{\langle \hat{\mathbf{e}}_k, \hat{\mathbf{e}}_k \rangle} \quad (26)$$

The overall QNILC iteration process is shown in Figure 4.

C. MONOTONIC CONVERGENCE ANALYSIS

The monotonic convergence of the QNILC with optimal learning gain is analyzed as follows:

Theorem: Define $\{\mathbf{e}_0, \mathbf{e}_1, \dots, \mathbf{e}_{k+1}, \dots\}$ as the tracking error sequence with QNILC method, which satisfies

$$\|\mathbf{e}_{k+1}\|^2 \leq \|\mathbf{e}_k\|^2 \quad (27)$$

Proof: The relation between \mathbf{e}_k and \mathbf{e}_{k+1} is

$$\begin{aligned} \mathbf{e}_{k+1} &= \mathbf{r} - \mathbf{G}\mathbf{u}_{k+1} \\ &= \mathbf{r} - \mathbf{G}(\mathbf{u}_k + \alpha_k \mathbf{d}_k) \\ &= \mathbf{r} - \mathbf{G}\mathbf{u}_k - \alpha_k \mathbf{G}\mathbf{d}_k \\ &= \mathbf{e}_k - \alpha_k \mathbf{G}\mathbf{d}_k \end{aligned} \quad (28)$$

$$\begin{aligned} \|\mathbf{e}_{k+1}\|^2 - \|\mathbf{e}_k\|^2 &= -\alpha_k \langle \mathbf{e}_k, \mathbf{G}\mathbf{d}_k \rangle - \alpha_k^* \langle \mathbf{G}\mathbf{d}_k, \mathbf{e}_k \rangle \\ &\quad + \alpha_k^* \alpha_k \langle \mathbf{G}\mathbf{d}_k, \mathbf{G}\mathbf{d}_k \rangle \end{aligned}$$

$$\begin{aligned} &= -\frac{\langle \mathbf{G}\mathbf{d}_k, \mathbf{e}_k \rangle \langle \mathbf{e}_k, \mathbf{G}\mathbf{d}_k \rangle}{\langle \mathbf{G}\mathbf{d}_k, \mathbf{G}\mathbf{d}_k \rangle} \\ &= -\frac{\|\mathbf{e}_k^H (\mathbf{G}\mathbf{d}_k)\|^2}{\|\mathbf{G}\mathbf{d}_k\|^2} \\ &= -\frac{\|\mathbf{e}_k^H \hat{\mathbf{e}}_k\|^2}{\|\hat{\mathbf{e}}_k\|^2} \leq 0 \end{aligned} \quad (29)$$

It is easy to conclude that the tracking error with the optimal iteration learning gain can converge monotonically. It is obviously irrelevant to the step size λ of estimating phase. To guarantee the convergence of estimating loop, the step size λ can be selected according to the tracking error. The update of the impedance matrix can reduce the modeling error gradually, which means that the step size λ can be set as a bigger value. But in this work, the estimating loop is seen as the auxiliary tool to attain the optimal learning gain, which is not considered as normal iteration step. Therefore, the step size $\lambda = 0.1$ is fixed in this work.

V. SIMULATION RESULTS AND DISCUSSION

To demonstrate the feasibility of the proposed algorithm, a comparable investigation is accomplished between the proposed QNILC algorithm and the classical ILC in automotive industry. In this section the simulation studies are performed with the a MIMO plant model with un-modeled dynamics. As shown in Figure 1, the front suspension test system uses force control for the lateral and longitudinal axes and displacement control for the vertical axis. For brevity, the vertical, lateral and longitudinal spindle forces are taken as responses of our interest, which brings forth a 3×3 system. In the system identification phase, the H_1 method is performed with $0 \sim 50$ Hz white-pink noise signals, where white noise for the low frequency range and pink noise for the higher range [3].

Figure 5 compares the experimental FRF matrix \hat{G} (blue solid) with the parametric model \tilde{G} (red dotted), which is derived by Recursive Least Squares (RELS) algorithm. In Figure 5, the columns signify inputs and the rows responses. Figure 5 (a) and (b) show the magnitude and phase frequency characteristics, respectively. It can be observed that the amplitude of the off-diagonal elements are lower than the diagonal elements, i.e. the cross-couplings are relatively weak.

The elements of parameter model \tilde{G} are given by

$$\tilde{G}_{11} = \frac{4.336e-5z^3 + 5.515e-3z^2 - 1.021e-2z + 5.121e-3}{z^5 - 4.372z^4 + 7.908z^3 - 7.392z^2 + 3.575z - 0.7183} \quad (30)$$

$$\tilde{G}_{21} = \frac{-0.00305z^3 + 0.009423z^2 - 0.008697z + 0.002325}{z^4 - 3.571z^3 + 4.837z^2 - 2.952z + 0.6863} \quad (31)$$

$$\tilde{G}_{31} = \frac{-0.04819z^3 + 0.1155z^2 - 0.1235z + 0.05019}{z^5 - 1.345z^4 + 0.6594z^3 + 0.9621z^2 - 0.223z - 0.4349} \quad (32)$$

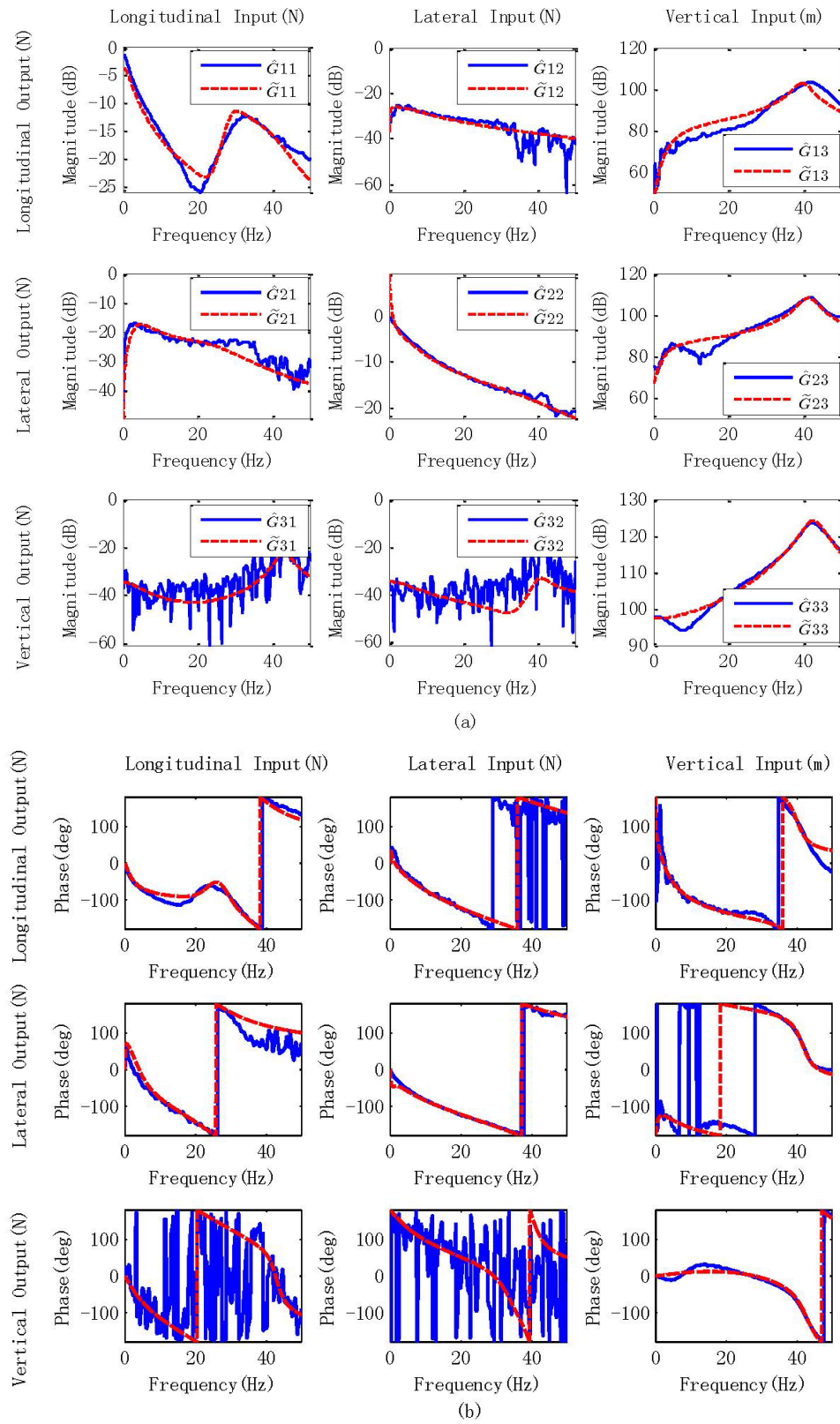


FIGURE 5. Experimental FRFs and parametric models of the multi-axial setup (a) magnitude characteristics (b) phase characteristics.

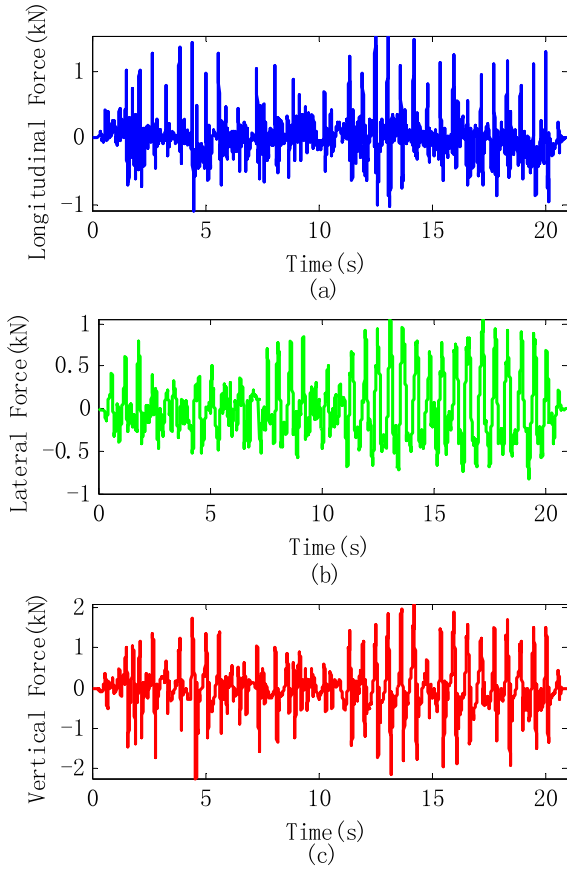


FIGURE 6. Target force signals for three different channels.

$$\tilde{G}_{12} = \frac{-0.0003999z^3 - 0.001462z^2 - 0.007173z - 0.005307}{z^5 - 2.022z^4 + 0.448z^3 + 1.567z^2 - 1.327z + 0.3343} \quad (33)$$

$$\tilde{G}_{22} = \frac{-1.236e - 2z^3 + 4.142e - 2z^2 - 2.642e - 2z - 2.347e - 3}{z^5 - 2.361z^4 + 1.065z^3 + 1.456z^2 - 1.633z - 0.4731} \quad (34)$$

$$\tilde{G}_{32} = \frac{-0.01252z^3 - 0.0125z^2 + 0.03551z - 0.01942}{z^5 - 1.703z^4 + 1.353z^3 + 0.832z^2 - 0.7277z - 0.08502} \quad (35)$$

$$\tilde{G}_{13} = \frac{-3469z^2 + 7010z - 3541}{z^4 - 3.519z^3 + 4.849z^2 - 3.094z + 0.7657} \quad (36)$$

$$\tilde{G}_{23} = \frac{7925z^2 - 27540z + 19530}{z^4 - 1.618z^3 - 0.1095z^2 + 1.635z - 0.8681} \quad (37)$$

$$\tilde{G}_{33} = \frac{2889z^2 + 16400z - 14370}{z^4 - 3.061z^3 + 3.902z^2 - 2.378z + 0.6038} \quad (38)$$

In order not to jeopardize the specimen, the performance of the QNILC will be validated with the MIMO parameter model $\tilde{\mathbf{G}}$ to replace the real physical plant \mathbf{G} . The FRF matrix $\tilde{\mathbf{G}}$ and $\tilde{\mathbf{G}}$ don't exactly coincide in all region in Figure 5, where the deviation can be seen as the modeling error.

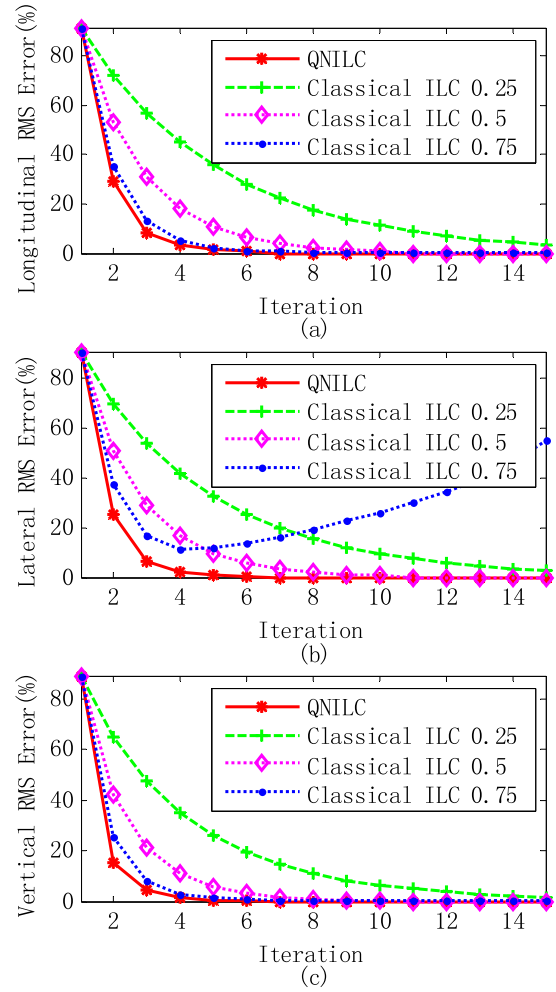


FIGURE 7. Relative RMS error comparison of QNILC and classical ILC.

TABLE 1. The iterative histories of QNILC and Classical ILC 0.5.

Iteration	Classical ILC 0.5			QNILC		
	Longitudinal channel	Lateral channel	Vertical channel	Longitudinal channel	Lateral channel	Vertical channel
k=0	91.57	90.66	88.96	91.57	90.66	88.96
k=1	53.40	51.05	42.12	29.52	25.21	15.19
k=2	31.20	29.03	21.09	8.05	6.44	4.45
k=3	18.21	16.65	10.84	3.15	2.07	1.20
k=4	10.64	9.64	5.67	1.54	0.68	0.42
k=5	6.25	5.65	3.02	0.75	0.41	0.14
k=6	3.69	3.34	1.64	0	0	0
k=7	2.21	1.98	0.93	0	0	0
k=8	1.35	1.18	0.56	0	0	0
k=9	0.84	0.71	0.36	0	0	0
k=10	0	0	0	0	0	0

As shown in Figure 6, a total length of 21s target signals with high amplitude are truncated from the road test signals, which is real-life spindle forces acquired from WFT.

The initial drive signals are created by multiplying the inverse of the FRF matrix with the target signals shown

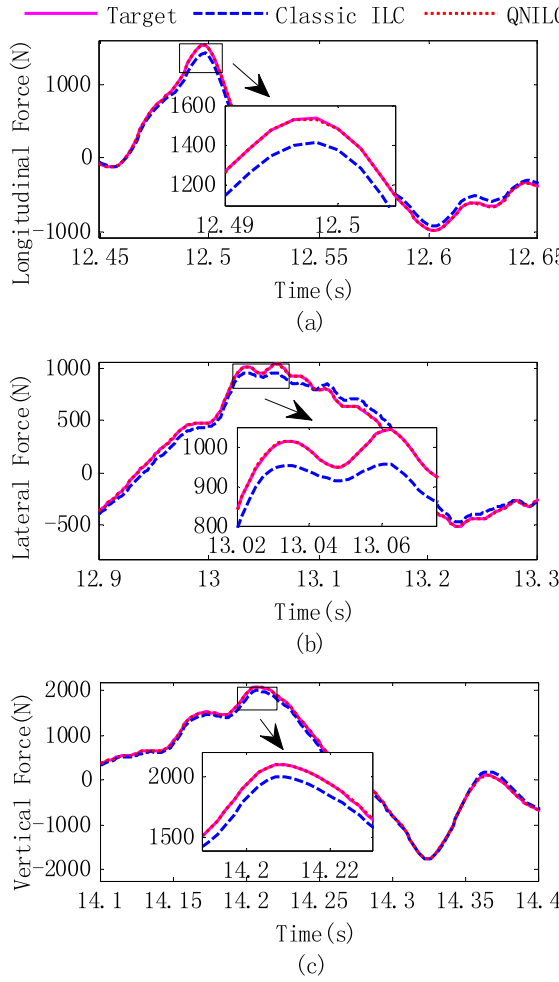


FIGURE 8. Response comparison of QNILC and classical ILC (after five iterations).

in Figure 4. But for safety reason, setting the first excitation level as 10% of the initial drive signal is considered in practice.

The relative Root Mean Square (RMS) error will be used as performance metrics to assess the convergence rate, which is

$$\varepsilon_{RMSi} = \frac{\sqrt{\sum_{k=0}^M \frac{[r_i(k)-y_i(k)]^2}{M}}}{\sqrt{\sum_{k=0}^M \frac{r_i^2(k)}{M}}} \times 100\% \quad (39)$$

where i is the channel number and M is the data length.

According to the relative RMS error comparison in Figure 7, it is observed that the iteration gain of the classical ILC becomes larger, the faster the convergence rate is. And a divergence occurs in the lateral channel if the gain in classical ILC reaches 0.75 in Figure 7 (b), which results by the modeling error and cross-coupling. It also can be seen that the proposed QNILC not only can guarantee the convergence

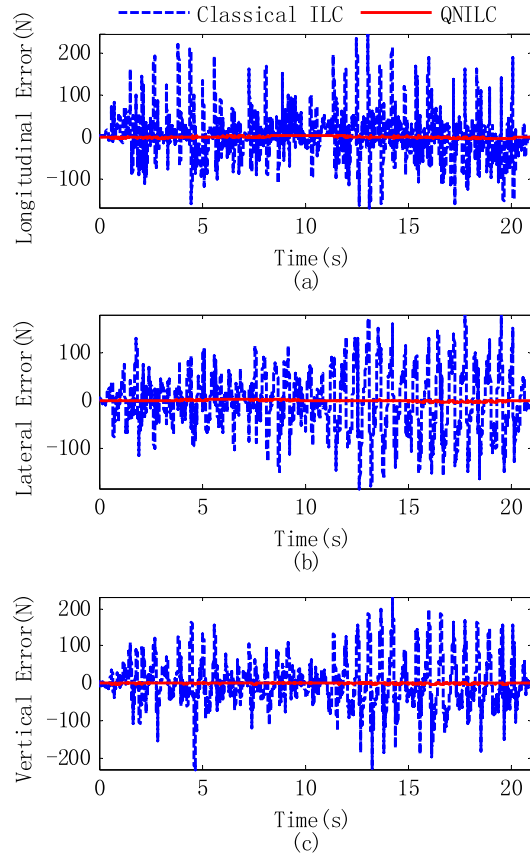


FIGURE 9. Tracking error comparison of QNILC and classical ILC (after five iterations).

of three channels but also converge faster than the classical ILC.

The values of relative RMS error of QNILC and Classical ILC with a 0.5 gain are listed in the Table I and the convergence threshold is set 1% for three channels. Obviously, the QNILC can reach a comparable accuracy with less iterations. The QNILC needs only five iterations to converge to the desirable index so it requires less time to obtain the drive file.

Consider that the classical ILC has a fixed learning gain of 0.5. Figure 8 compares the responses of two methods after 5 iterations with target time waveforms. It can be observed that the curve with QNILC can match the target signal better, especially at the peak force point. The corresponding error results are displayed in Figure 9. It is evident that the errors with the QNILC are much smaller than those with the classical ILC during the same iterations.

The Power Spectral Density (PSD) also provides useful insights, as shown in Figure 10. The energy is concentrated on the frequency band 0~15Hz. Over the entire frequency range, the PSD with QNILC matches the target PSD. Generally, the peak PSD has a more influence on the damage ratio of the specimen. It can be seen that the PSD with the QNILC method is consistent with the target at the peak value of three channels. As a consequence, the QNILC allows a

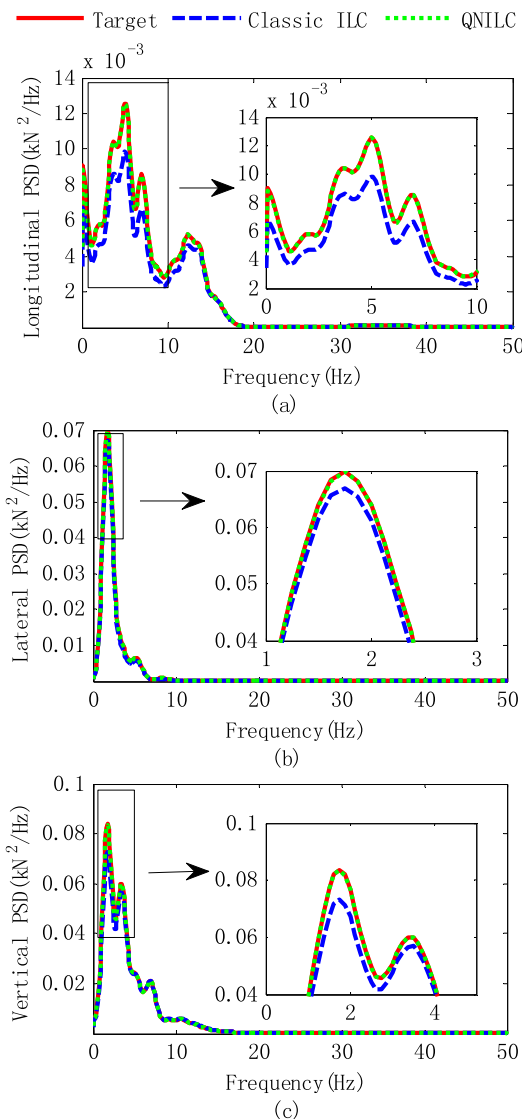


FIGURE 10. Response power spectra comparison of QNILC and classical ILC (after five iterations).

more accurate replication of the target signals with the same iterations.

VI. CONCLUSION

A QNILC scheme with optimal iteration gain is proposed to accelerate the convergence rate of iteration procedure for generating the drive file in automotive durability testing. The update of the impedance matrix with Broyden's method can make the iteration more robust. An optimal iteration gain can be derived from the auxiliary estimating loop readily. With this optimal iteration gain, the QNILC can keep the iteration converging monotonically. The QNILC can be implemented more easily without manual gain adjustment. The proposed approach towards MIMO system has been investigated through simulation. Simulation results demonstrate that the QNILC can reach a comparable tracking accuracy with less iterations. Compared to recent parametric model based

ILC, the proposed method can easily extend to larger numbers of channels (e.g. the full-vehicle durability testing) to replace the classical ILC. The physical multi-axial road test rig is under construction and the practical application of QNILC will be pursued.

ACKNOWLEDGMENT

The authors would like to thank the associate editor and the reviewers for their careful reading and constructive comments. They appreciate Guang Yang from China Automotive Technology and Research Center (CATARC) to collect the experimental data.

REFERENCES

- [1] C. J. Dodds and A. R. Plummer, "Laboratory road simulation for full vehicle testing: A review," SAE Technical Paper 2001-26-0047, 2001.
- [2] J. W. Kim, D. J. Xuan, and Y.-B. Kim, "Robust control application for a three-axis road simulator," *J. Mech. Sci. Technol.*, vol. 25, no. 1, pp. 221–231, 2011.
- [3] J. De Cuyper, D. Coppens, C. Lefooghe, J. Swevers, and M. Verhaegen, "Advanced drive file development methods for improved service load simulation on multi axial durability test rigs," in *Proc. Acoust. Vibrat. Asia*, 1998, pp. 339–354.
- [4] D. Chindamo, M. Gadola, and F. P. Marchesin, "Reproduction of real-world road profiles on a four-poster rig for indoor vehicle chassis and suspension durability testing," *Adv. Mech. Eng.*, vol. 9, no. 8, pp. 1–10, 2017.
- [5] H. Yudong, Z. Hong, and X. Gang, "Study on control algorithm of the electro-hydraulic servo system for load simulation test," in *Future Communication, Computing, Control and Management*. Berlin, Germany: Springer, 2012, pp. 533–541.
- [6] B. Cornelis, A. Toso, W. Verpoest, and B. Peeters, "Improved MIMO FRF estimation and model updating for robust Time Waveform Replication on durability test rigs," in *Proc. Int. Conf. Noise Vibrat. Eng.*, vol. 1, 2014, pp. 759–774.
- [7] A. Bhattacharya, N. Malik, and S. Jindal, "Optimization of simulation channels for inverse FRF calculation on 6-axis road load simulator: An experimental approach," SAE Technical Paper 2017-26-0303, 2017.
- [8] B. Cornelis, A. Toso, W. Verpoest, and B. Peeters, "Adaptive modelling for improved control in durability test rigs," in *Proc. 20th Int. Congr. Sound Vibrat.*, 2013, pp. 507–516.
- [9] U. Musella, S. Manzato, B. Peeters, and P. Guillaume, "CR-Calculus and adaptive array theory applied to MIMO random vibration control tests," *J. Phys., Conf. Ser.*, vol. 744, no. 1, 2016, Art. no. 012175.
- [10] A. D. Raath, "A new time domain parametric dynamic system identification approach to multiaxial service load simulation testing in components," *Int. J. Fatigue*, vol. 19, no. 5, pp. 409–414, 1997.
- [11] J. De Cuyper and M. Verhaegen, "State space modeling and stable dynamic inversion for trajectory tracking on an industrial seat test rig," *J. Vib. Control*, vol. 8, no. 7, pp. 1033–1050, 2002.
- [12] U. Dursun and T. Bayram, "Tracking control solution for road simulators: Model-based iterative learning control approach improved by time-domain modelling," *Gazi Univ. J. Sci.*, vol. 25, no. 2, pp. 435–446, 2012.
- [13] T. Müller, J. Ziegmann, S. Krüner, and C. Endisch, "Optimization of inverse model identification for multi-axial test rig control," in *Proc. MATEC Web Conf.*, vol. 42, 2016, p. 01002.
- [14] T. Müller, U. Vögele, and C. Endisch, "Disturbance compensation for iterative control of suspension durability test rigs," in *Proc. IEEE Int. Conf. Adv. Intell. Mechatron. (AIM)*, Jul. 2016, pp. 1675–1681.
- [15] T. Müller and C. Endisch, "Compensation techniques for iterative rig control in multi-axial durability testing," in *Proc. IEEE 21st Int. Conf. Emerg. Technol. Factory Automat. (ETFA)*, Sep. 2016, pp. 1–7.
- [16] S. Moten, G. Pipeleers, W. Desmet, and J. Swevers, "A combined use of the adaptive inverse plant modeling and iterative learning control strategy for service load simulations," in *Proc. 5th Austral. Control Conf. (AUCC)*, Nov. 2015, pp. 277–282.

- [17] M. Volckaert, A. Van Mulders, J. Schoukens, M. Diehl, and J. Swevers, "Model based nonlinear iterative learning control: A constrained Gauss-Newton approach," in *Proc. 17th Medit. Conf. Control Automat.*, Jun. 2009, pp. 718–723.
- [18] G. Xu, J. Y. Zhou, and H. Zhou, "A new Nonlinear Iterative learning controller for road simulator," *Appl. Mech. Mater.*, vols. 373–375, pp. 1546–1550, Aug. 2013.
- [19] G. Xu, M. Volckaert, J. Swevers, and H. Zhou, "Moving horizon model inversion for nonlinear ILC," *Key Eng. Mater.*, vol. 460, pp. 184–189, Jan. 2011.
- [20] J. J. A. Eksteen and P. S. Heyns, "An alternative update formula for non-linear model-based iterative learning control," *Inverse Problems Sci. Eng.*, vol. 24, no. 5, pp. 860–888, 2016.
- [21] J. De Cuyper, "Linear feedback control for durability test rigs in the automotive industry," Ph.D. dissertation, Dept. Mechan. Eng., Catholic Univ. Leuven, Leuven, Belgium, 2006.
- [22] J. De Cuyper, M. Verhaegen, and J. Swevers, "Off-line feed-forward and H_∞ feedback control on a vibration rig," *Control Eng. Pract.*, vol. 11, no. 2, pp. 129–140, 2003.
- [23] Y. Tang, G. Shen, Z. C. Zhu, and C. F. Yang, "Time waveform replication for electro-hydraulic shaking table incorporating off-line iterative learning control and modified internal model control," *Proc. Inst. Mech. Eng. I. J. Syst. Control Eng.*, vol. 228, no. 9, pp. 722–733, 2014.
- [24] D. H. Owens, "Multivariable norm optimal and parameter optimal iterative learning control: A unified formulation," *Int. J. Control.*, vol. 85, no. 8, pp. 1010–1025, 2012.
- [25] D. H. Owens, B. Chu, and M. Songjun, "Parameter-optimal iterative learning control using polynomial representations of the inverse plant," *Int. J. Control.*, vol. 85, no. 5, pp. 533–544, 2012.
- [26] T. Lin and D. H. Owens, "Monotonic Newton method based ILC with parameter optimization for non-linear systems," *Int. J. Control.*, vol. 80, no. 8, pp. 1291–1298, 2007.
- [27] H.-F. Tao, W. Paszke, E. Rogers, K. Gałkowski, and H. Yang, "Modified Newton method based iterative learning control design for discrete non-linear systems with constraints," *Syst. Control Lett.*, vol. 118, pp. 35–43, Aug. 2018.
- [28] Y. Geng and X. Ruan, "Quasi-Newton-type optimized iterative learning control for discrete linear time invariant systems," *Control Theory Technol.*, vol. 13, no. 3, pp. 256–265, 2015.
- [29] X. Wang, D. Cong, Z. Yang, S. Xu, and J. Han, "Iterative learning control with complex conjugate gradient optimization algorithm for multiaxial road durability test rig," *Proc. Inst. Mech. Eng. C. J. Mech. Eng. Sci.*, to be published. doi: [10.1177/0954406218786981](https://doi.org/10.1177/0954406218786981).
- [30] J. M. Martínez, "Practical quasi-Newton methods for solving nonlinear systems," *J. Comput. Appl. Math.*, vol. 124, nos. 1–2, pp. 97–121, Dec. 2000.
- [31] S. Zhang and Y. Xia, "Solving nonlinear optimization problems of real functions in complex variables by complex-valued iterative methods," *IEEE Trans. Cybern.*, vol. 48, no. 1, pp. 277–287, Jan. 2018.
- [32] N. C. Hay and D. E. Roberts, "Road simulators: The iterative algorithm for drive file creation," SAE Technical Paper, 2006.
- [33] L. Sorber, M. Van Barel, and L. De Lathauwer, "Unconstrained optimization of real functions in complex variables," *SIAM J. Optim.*, vol. 22, no. 3, pp. 879–898, 2012.
- [34] H. Li and T. Adali, "Optimization in the complex domain for nonlinear adaptive filtering," in *Proc. 14th Asilomar Conf. Signals. Syst. Comput.*, Pacific Grove, CA, USA, Oct./Nov. 2006, pp. 263–267.
- [35] K. Kreutz-Delgado. (Jun. 2009). "The complex gradient operator and the CR-calculus." [Online]. Available: <https://arxiv.org/abs/0906.4835>
- [36] A. van den Bos, "Complex gradient and Hessian," *IEE Proc. Vis., Image Signal Process.*, vol. 141, no. 6, pp. 380–383, Dec. 1994.
- [37] D. E. Roberts and N. C. Hay, "Dynamic response simulation for a nonlinear system," *J. Sound Vib.*, vol. 281, nos. 3–5, pp. 783–798, Mar. 2005.
- [38] C. G. Broyden, "A class of methods for solving nonlinear simultaneous equations," *Math. Comput.*, vol. 19, no. 92, pp. 577–593, Oct. 1965.
- [39] M. A. Gomes-Ruggiero, J. M. Martínez, and A. C. Moretti, "Comparing algorithms for solving sparse nonlinear systems of equations," *SIAM J. Sci. Stat. Comput.*, vol. 13, no. 2, pp. 459–483, Mar. 1992.
- [40] M. A. Underwood, "Adaptive control method for multi-exciter sine tests," U.S. Patent 5 299 459, Apr. 1994.



XIAO WANG received the B.E. degree in mechatronics engineering from Shandong Jianzhu University, Jinan, China, in 2011, and the M.S. degree from the Dalian University of Technology, Dalian, China, in 2014. He is currently pursuing the Ph.D. degree with the Harbin Institute of Technology, Harbin, China. His research interests include electro-hydraulic servo control, adaptive inverse control, and iterative learning control.



DACHENG CONG received the Ph.D. degree in instrument science and technology from the Harbin Institute of Technology, Harbin, China, in 2002, where he has been an Associate Professor and a Professor with the Department of Mechatronics Engineering, since 2003 and since 2008, respectively. He is currently a Deputy Director of the Institute of Simulation and Test of ElectroHydraulic Servo System. He has headed over 20 national, provincial, and industrial projects which include the 863 Project, the National High and New Project, and the National 921 Engineering Project. He has authored or co-authored over 50 journal and conference articles. His main research interests include six-DOF shaking table's vibration control, six-DOF motion simulation control systems, and three-stage servo valve control technique with large flow and high response. He is a member of the Fluid Power Transmission and Control Association and China Ordnance Society. He received the National Science and Technology Progress Award, Second Prize, in 2009.



ZHIDONG YANG received the Ph.D. degree in mechatronics engineering from the Harbin Institute of Technology, Harbin, China, in 2009, where he has been a Lecturer and an Associate Professor with the Department of Mechatronics Engineering, since 2010 and since 2015, respectively. He has headed or taken part in the two National Science Foundations for Distinguished Young Scholars of China and published many articles. He has headed over ten national, provincial, and industrial projects and developed the multi-function real-time prototype control system software. His main research interests include redundant-driven electro-hydraulic shaking table control, inner force coupling analysis and control, adaptive control, and model control.



SHENGJIE XU received the B.S. degree in automotive engineering from the Hebei University of Technology, Tianjin, China, in 2011. Since 2011, he has been a Road Simulation Test Engineer with China Automotive Technology and Research Center, his career started from vehicle on-road testing; then, he dive into the field of road load data acquisition and road simulation. His research interests include RLDA instrumentation and data analysis, vehicle component transduction, full vehicle road simulation testing (remote parameter control), proving ground correlation, and system identification.



JUNWEI HAN received the Ph.D. degree in mechatronics engineering from the Harbin Institute of Technology, Harbin, China, in 1992. In 1992, he was a Researcher with the China Earthquake Administration Institute of Engineering Mechanics and a Researcher with Mechanical Engineering Post-Doctoral Mobile Stations, Harbin Industrial University, in 1994. Since 1997, he has been a Professor with the Department of Mechatronics Engineering, Harbin Institute of Technology. He is currently the Academic Leader of fluid power transmission and control and the Director of the Institute of Simulation and Test of Electro-Hydraulic Servo System and the National State Key Laboratory

of Robotics and System. He has headed over 30 national, provincial, and industrial projects. He has authored or co-authored over 180 journal and conference articles. His main research interests include electro-hydraulic servo control, redundant-driven parallel control and flight simulation and simulation test systems, six-DOF shaking table's vibration control, six-DOF motion simulation control systems, and three-stage servo valve control technique with large flow and high response. He is a member of the Fluid Power Transmission and Control Association and a Council Member of the China Ordnance Society. He honored the Ministry of Education in the new Century Excellent Talents and the Defense Industry Young and Middle-Aged Expert with Outstanding Contributions. He received the National Science and Technology Progress Award First Prize and Second Prize.

• • •